Carbon 192 (2022) 234–248

Contents lists available at ScienceDirect

Carbon

journal homepage: www.elsevier.com/locate/carbon

Ultrasensitive and highly stretchable sensors for human motion monitoring made of graphene reinforced polydimethylsiloxane: Electromechanical and complex impedance sensing performance

Antonio del Bosque *, Xoan F. Sánchez-Romate , María Sánchez , Alejandro Ureña

Materials Science and Engineering Area, Escuela Superior de Ciencias Experimentales y Tecnología, Universidad Rey Juan Carlos, C/Tulipán s/n, 28933, Móstoles, Spain

ARTICLE INFO

Article history:
Received 30 August 2021
Received in revised form
4 February 2022
Accepted 18 February 2022
Available online 24 February 2022

Keywords:
Graphene nanoplatelets
Wearable sensors
EIS
Human motion monitoring
SHM

ABSTRACT

Highly stretchable sensors based on graphene nanoplatelet (GNP) reinforced polydimethylsiloxane (PDMS) are manufactured for human motion monitoring purposes. The strain sensing analysis shows ultra-high gauge factor (GF) values from 40 to 300 at low strain levels up to 10^6 at high deformations at tensile conditions, and a decreasing sensitivity as GNP content increases. The compressive behavior shows an initial decrease of the electrical resistance, due to the prevalence of in-plane mechanisms, followed by a stable increase, due to the prevalence of out-of-plane mechanisms. In this regard, the Electrical Impedance Spectroscopy (EIS) analysis shows an increase of the complex impedance with increasing compressive strain. The equivalent RC-LRC circuit allows to explain the electrical mechanisms governing the compressive behavior, where the LRC element denotes the contact and intrinsic resistance and the RC element the tunnelling effect. Finally, a proof of concept of human motion monitoring proves the capability of the scalable and easy-manufactured sensors to detect frowning, raising eyebrows, blinking, breathing, blowing and, even, vocal cord motion, where each phoneme follows a unique pattern, with a robust electrical response.

1. Introduction

Nowadays, the use of flexible wearable sensors for human motion monitoring is gaining a great deal of attention. One of the most common types of flexible and stretchable strain sensors is based on the use of carbon nanoparticles as reinforcement in polymer matrices [1,2]. The basis for the development of these kind of sensors lies in the physical principle that the addition of carbon nanoparticles into these insulating systems allows the creation of percolating electrical networks, promoting the enhancement of the electrical conductivity [3]. In fact, the determination of the percolation threshold in these nanocomposites, that is defined as the volume fraction where the insulating material becomes electrically conductive, has attracted the attention of numerous researchers as it is a key parameter of the electrical properties. For example, the percolation threshold for carbon black (CB) usually is in the range from 2 to 10%, for carbon nanotubes (CNTs), around 0.05–6% and for graphene nanoplatelets (GNPs), 2–12%, depending on the geometry of the nanofiller and the dispersion procedure [4]. In these types of systems, the electrical properties are governed by three mechanisms: the intrinsic resistivity of carbon nanoparticles, the contact resistance between adjacent nanoparticles and the tunnelling effect between neighbouring ones. Thereby, when these nanocomposites are subjected to strain, the distance between adjacent nanoparticles and surfaces in contact between overlying ones are modified, causing changes in the global conductivity of the material as the electrical resistance associated to contact and tunnelling effect is also modified [5–7]. Therefore, these facts, in combination with the intrinsic piezoresistive response of the carbon nanofillers, make these nanocomposites very sensitive to mechanical deformations.

In recent years, developments that use different materials have been widely studied with the aim of obtaining flexible and stretchable sensors with a high Gauge Factor (GF), defined as the change of the electrical resistance divided by the applied strain, manufacturing by low cost and easy-scalable process. Some studies dealt with the manufacturing of thin graphene films deposited uniformly on the polydimethylsiloxane (PDMS) surface using

* Corresponding author.
E-mail address: antonio.delbosque@urjc.es (A. Bosque).

https://doi.org/10.1016/j.carbon.2022.02.043

different techniques such as spraying or CVD, showing a GF of around 10^3 and a failure strain up to 25% [8–10]. Eco-flex-based resistive type sensors reinforced with CNTs showed GF of 1–18 with a linear response [11–13]. Moreover, CNTs/PDMS exhibited a strain range of more than 40% and high stability, but a low GF (between 5 and 8) [14,15]. Furthermore, the electromechanical response of an epoxy resin poly(ethylene glycol) diglycidyl ether reinforced with CNTs was also studied and its application for human motion sensing was proved, although the GF values obtained at low deformations were not so high (below 10) [16]. Alternatively, CB was used in PDMS in a film form, but it presented lower stretchability and GF than sensors based in CNTs/graphene [17–19]. The main reason for the different GF depending the carbon nanoparticle lies in the fact that the 2D nature of graphene promotes a higher tunnelling area between neighbouring nanoparticles so the interparticle distance can be increased and, thus, the sensitivity in comparison to 1D or 0D nanoparticles [20]. On the other hand, natural rubbers or thermoplastic elastomer have been also commonly used as polymer matrix or support of strain sensors [21–28]. In every case, they have proved their potential for sensing applications, although the detection of small strain with a repeatable pattern remains to be investigated.

Therefore, this work is focused on the development of highly stretchable and ultrasensitive strain sensors for the detection of small human movements based on PDMS reinforced with GNPs. In this regard, the electromechanical and Electrical Impedance Spectroscopy (EIS) analysis have been explored, following a scalable and easy-manufactured process. The electromechanical analysis allowed to determine the sensitivity of the electrical response under applied strain, whereas EIS analysis gave a deeper knowledge about the electrical mechanisms that governs the electrical properties of the manufactured nanocomposites. The electromechanical response was carried out under tensile and compressive strain. The EIS analysis was carried out on pristine and under compressive conditions to demonstrate the complex impedance sensitivity to mechanical deformation. Finally, a proof of concept of human motion monitoring was also carried out from large to very small strains to validate the applicability of the developed materials.

2. Experimental

2.1. Materials

Nanocomposites were manufactured with GNPs embedded in a silicone elastomer. GNPs were supplied by XG-Science® with a commercial name M25. They have an average lateral size of 25 μm, a thickness of 6 nm, and an electrical conductivity of ~10^7 S/m parallel to the surface and ~10^2 S/m in the transversal direction. Silicone elastomer was Polydimethylsiloxane (PDMS) with a commercial formula called SYLGARD 184TM supplied by Dow®, which was manufactured using a mixing ratio of 10:1 between the monomer and the curing agent. The monomer has a viscosity of 5100 mPa s at room temperature and the mixture between the monomer and the curing agent has a viscosity of 3500 mPa s.

2.2. Manufacturing of GNP reinforced PDMS sensors

GNP/PDMS nanocomposites were manufactured with 4, 6, 8 and 10 wt% GNPs. The contents were selected to be slightly above the percolation threshold. GNPs were dispersed in the polymer matrix by three roll milling (3RM) process. It consisted in a progressive reduction of the gaps between consecutive rolls rotating at different speeds in a proportion 1:3:9, where the last roll rotated at 250 rpm. This process induces high shear forces on the mixture to disaggregate GNP agglomerates. The parameters of the 3RM process were based on a previous study [29], and it consisted of a single cycle with a 120 μm gap first roll and 40 μm gap last roll as it was proved that increasing number of cycles promoted a possible damage in the nanoparticles.

Following the dispersion procedure, the mixtures were degasified under vacuum conditions in a magnetic stirrer during 10 min at 100 °C to removing the possible entrapped air. After that, the curing agent was added in 10:1 proportion and mixed at room temperature. Finally, the mixture was poured in the corresponding steel mold previously smeared with two layers of release agent (Frekote 700NC LOCTITE®) and they were cured in an oven at 125 °C to 20 min, as indicated in the commercial silicone elastomer data sheet.

2.3. Microstructural characterization

To evaluate the dispersion state reached for GNP/PDMS with these processing, the fracture surfaces under cryogenic conditions were analyzed by means of Scanning Electron Microscopy (SEM) using a S–3400N machine from Hitachi. The nanocomposite cryofractures were coated by a thin layer of gold for a proper characterization.

2.4. Electrical conductivity measurements

The electrical conductivity was evaluated using a Source Meter Unit instrument (Keithley 2410). It was determined by calculating the slope of the current-voltage curve at 0–100 V for 4 and 6 wt% GNP and at 0–15 V for 8 and 10 wt% GNP, due to the higher conductivity expected in the last ones. For these experiments, three samples with 60 × 20 × 3 mm^3 dimensions were tested. Four electrodes made of copper wires were attached with silver ink to the sample to make a four-probe measurement. This schematic configuration is shown in Fig. 1a.

2.5. Electromechanical tests of GNP/PDMS strain gauges

The strain monitoring capabilities of GNP/PDMS materials were analyzed in tensile and compression tests. These tests were carried out in a universal testing machine Zwick Z100 with a load cell of 500 N. On one hand, four tensile specimens of each condition were analyzed accordingly to ISO 527–1:2019, specifically, at a test rate of 10 mm/min. On the other hand, at least two compression specimens of each GNP content with 30 × 20 × 12 mm^3 dimensions were tested with a preload of 1 N and at a test rate of 1 mm/min.

Simultaneously to the mechanical tests, the electrical resistance was recorded using a digital multimeter Agilent DMM 34410A. In case of tensile test, two electrodes made of copper wires were attached around the nanocomposite surface in the center of the sample at 30 mm, using conductive silver ink to minimize the contact resistance, as shown Fig. 1b. For compression test, the copper electrodes were attached with silver ink to the upper and lower sample surfaces, as can be seen in Fig. 1c.

These tests allowed to determine the Gauge Factor (GF), that can be defined, as commented before, as the normalized resistance change ($\Delta R/R_0$) divided by the applied strain (ε), as shown in equation (1):

$$GF = \frac{\Delta R/R_0}{\varepsilon} \quad (1)$$

Moreover, in order to study an electrical stable repeatability, GNP/PDMS tensile and compression specimens were subjected to continuous bending and releasing for 200 cycles up to 1% strain level, at a fixed rate of 15 mm/min.

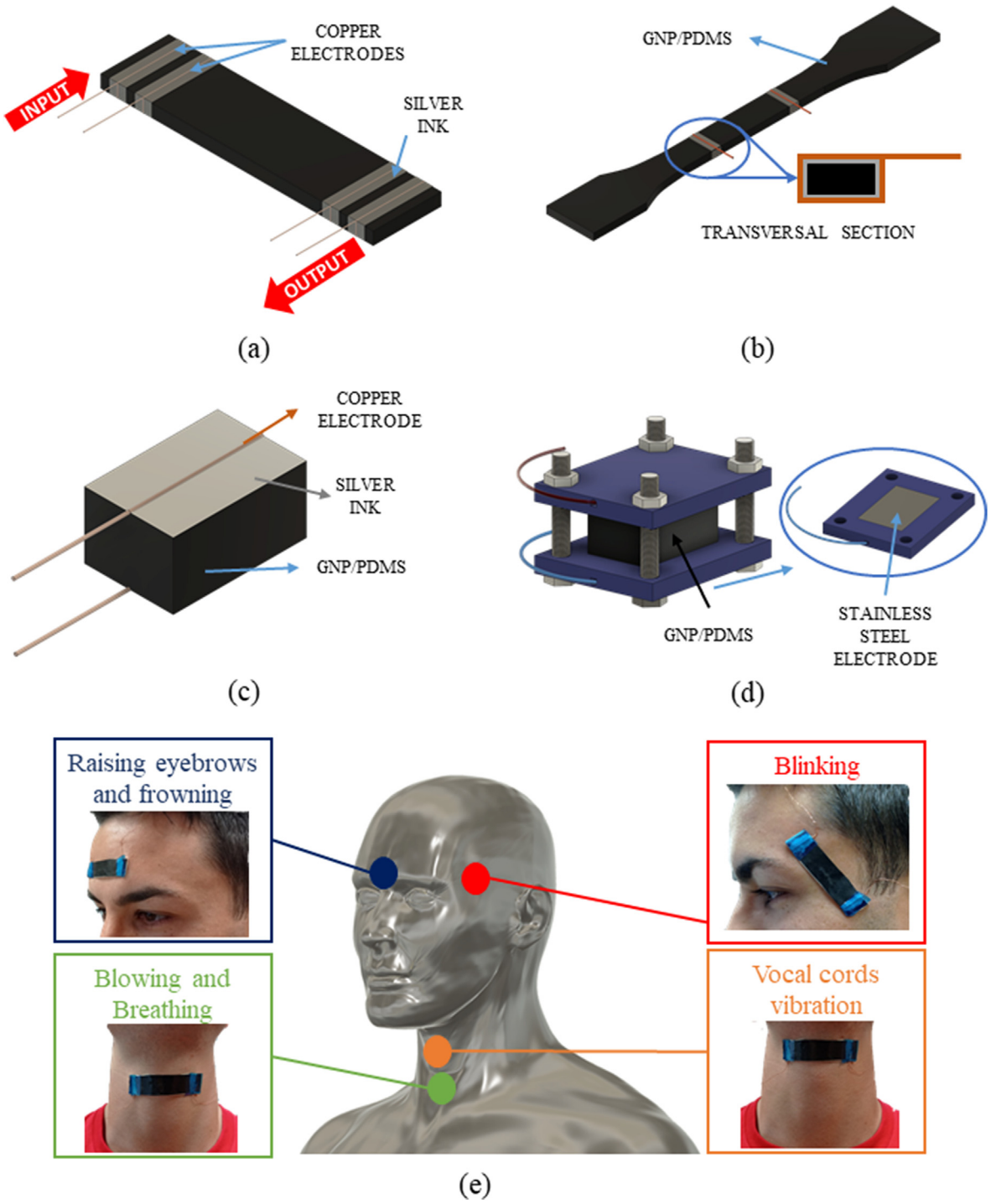

Fig. 1. Schematics of electrode's disposition in (a) conductivity measurements, (b) tensile and (c) compression test for strain monitoring characterization, (d) EIS measurements and (e) proof of concept of human motion monitoring. (A colour version of this figure can be viewed online.)

2.6. Electrical Impedance Spectroscopy (EIS)

The Electrical Impedance Spectroscopy (EIS) response was studied by analyzing the $30 \times 20 \times 12$ mm^3 samples in an AUTOLAB PGSTAT302 N potentiostat. The samples were sandwiched between two symmetric clean and polished stainless-steel electrodes and introduced in a pressure cell to guarantee and control the distance between de two electrodes, that is, the strain level of the nanocomposite, as can be seen in Fig. 1d. The nanocomposite area in contact with the stainless-steel electrodes was painted with silver ink with the aim of enhancing the electrode-nanocomposite contact.

The AC impedance of the samples was measured at room temperature using a frequency range between 1 MHz and 100 Hz and an amplitude of 30 mV. Three measurements were analyzed applying pressure with the cell to each nanocomposite, which it was quantitatively evaluated by three distances between the electrodes (9, 10.5 and 12 mm, approximately). Finally, the Nyquist

plots (imaginary contribution of impedance Z" vs real contribution Z') were fitted to an equivalent circuit to explain the physical meaning of the system.

2.7. Proof of concept

To analyze the viability in human motion monitoring applications, two 6 wt% GNP sensors with 65 × 16 × 1 mm^3 and 40 × 12 × 1 mm^3 dimensions with copper electrodes attachments were used by fixing nanocomposites on a human neck and face (Fig. 1e) with an adhesive layer, as a proof of concept. Specifically, monitoring vocals cords vibration (spelling vowels), blinking, blowing, breathing, frowning, and raising eyebrows movements.

3. Results and discussion

3.1. Electrical conductivity measurements

Electrical conductivity measurements are summarized in Fig. 2. It can be observed that an increasing in the GNP content leads, as expected, to an increase of the electrical conductivity of the nanocomposites; explained by the increasing number of electrical pathways. Furthermore, the electrical conductivity results proved that the percolation threshold, that is, the minimum GNP fraction that allows the creation of electrical pathways was less than 4 wt%.

On the other hand, when comparing the results with other studies using epoxy systems and the same nanoparticles, but dispersed by ultrasonication, it can be observed that, at low GNP contents (4 and 6 wt%), the electrical conductivity values are considerably higher [30,31].This is explained by the positive effect of three roll milling process, that induces a much lower breakage effect over the nanoparticles than ultrasonication technique. In fact, it has been observed that the modification of the three-roll milling process with one cycle leads, also, to a lower breakage of the nanoparticles themselves, resulting in a more efficient electrical network than other methods with a progressive reduction of the gap between rolls in subsequent cycles [29]. Therefore, the proposed method provides a good dispersion combined with a low breakage of GNPs.

The good GNP dispersion was also confirmed by the SEM analysis of cryofracture surfaces. Fig. 3 shows a homogeneous distribution of nanoparticles in the samples with different GNP contents, where the nanoparticles are marked with red arrows. Here, it can be observed that, by increasing the GNP content, the number of nanoparticles observed in the fracture surfaces is higher, as well as their tendency to form aggregates (Fig. 3f and h). However, in any case, there are no significant agglomerates in the samples, which explains the high efficiency of the electrical network generated.

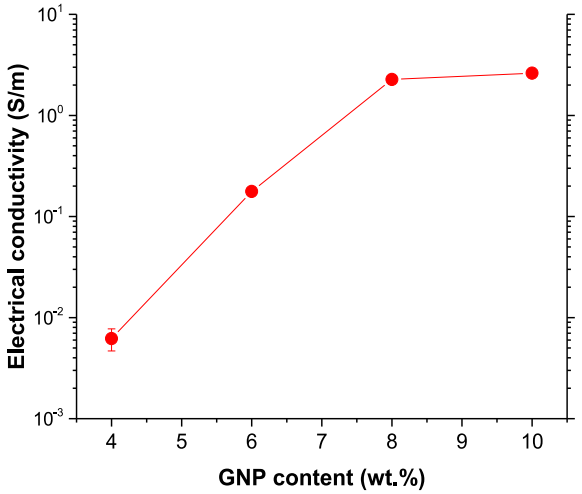

Fig. 2. Electrical conductivity measurements of GNP nanocomposites. (A colour version of this figure can be viewed online.)

3.2. Electromechanical response

Some examples of the electromechanical response under tensile load are shown in the graphs of Fig. 4a. Here, some interesting facts can be stated. On one hand, a very pronounced exponential electrical response can be observed with the applied strain. This is mainly attributed to the tunnelling effect between adjacent nanoparticles, that, accordingly to the well-known Simmons' formula [32], follows a linear-exponential behaviour. In this case, this exponential behaviour with the applied strain is more prevalent, due to the 2D nature of the nanoparticles. More specifically, the tunnelling area between adjacent GNPs is much larger than in the case of CNTs. Therefore, the minimum distance between adjacent nanoparticles to guarantee a tunnelling effect can be increased in comparison to CNTs, leading to a more prevalent exponential response.

In this type of sensors, it is important to analyze the influence of GNP in mechanical properties, but more specifically in the maximum values of strain, as is widely discussed in Supplementary Information. Here, the nanocomposite that contains 6 wt% GNP reached a maximum strain level similar to neat PDMS (around 70%), but a reduction of more than 40% in this property for 8 and 10 wt% GNP is reported, as reported in the Supplementary Information (Figs. S1 and S2).

On the other hand, the very high failure strain values also lead to a higher prevalence of exponential effects during the mechanical test. In this regard, only the 8 and 10 wt% GNP samples are able to monitor all the mechanical tests, whereas the samples at 6 and 4 wt % GNP experienced a loss of electrical contact at 1.5 and 15% strain, respectively, as can be observed in the detailed graphs at low strain levels of Fig. 4b.

In this regard, a detriment of 20% in the tensile strength is observed when GNP are introduced. Moreover, a reduction of more than 40% in strain at failure for 8 and 10 wt% GNP is reported, that is not appreciated for 4 and 6 wt% GNP. Thus, the nanocomposite that contains 6 wt% GNP reached a maximum strain similar to neat PDMS, which reinforces the reasons for using this sensor as optimal.

In this regard, the graph of Fig. 4c show the GF values as a function of applied strain for the different conditions. As commented before, the electrical sensitivity increased with the applied strain due to the exponential behaviour of the electrical response. More specifically, the GNP doped PDMS sensors showed high values of GF at low strain levels (from 40 to 300 at $\varepsilon = 2.5\%$) and an ultrasensitive response at high strain levels (around 10^6 at $\varepsilon = 40\%$), five or six orders of magnitude above conventional metallic gauges. In particular, the 6 wt% GNP sensors, showed an ultrasensitive response also at relative low strain levels (GF of around 10^6 at $\varepsilon = 10\%$). As commented before, these GF values are much higher than similar sensors reinforced with CNTs [16], due to the 2D nature of the GNPs, which a much more pronounced exponential behavior of the electrical resistance with the applied strain.

In addition, by analysing the effect of GNP content, it can be observed that an increase in the GNP amount leads to a decrease of the GF, due to the lower distance between adjacent nanoparticles which induces a lower variation of the electrical resistance. Therefore, as expected, the closer to the percolation threshold, the higher the sensitivity of the system, although the loss of electrical contact also takes places earlier.

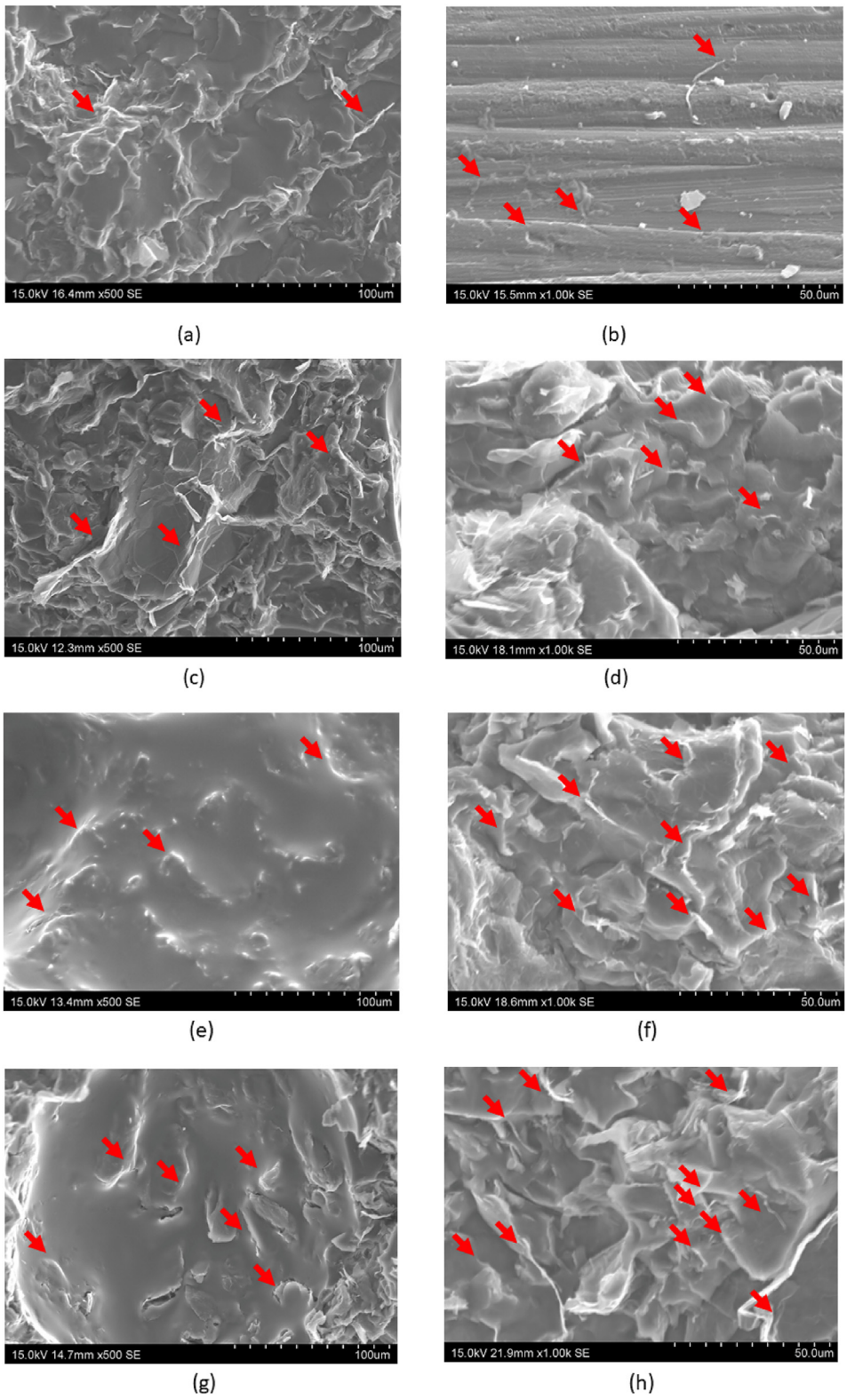

Fig. 3. SEM images of fracture surfaces of (a–b) 4, (c–d) 6, (e–f) 8 and (g–h) 10 wt% GNP samples where the red arrows denote the presence of GNPs. (A colour version of this figure can be viewed online.)

Fig. 5a summarizes the electromechanical response under compression load. Here, an initial decrease of the electrical resistance is observed, followed by an exponential increase, as can be observed in the detailed graphs. This fact was previously described [20,33], and can be easily explained by the interactions that take part between nanoparticles correlated to the mechanical response of the sample during the compression test (schematics of Fig. 5b).

The initial decrease is associated to the in-plane mechanisms

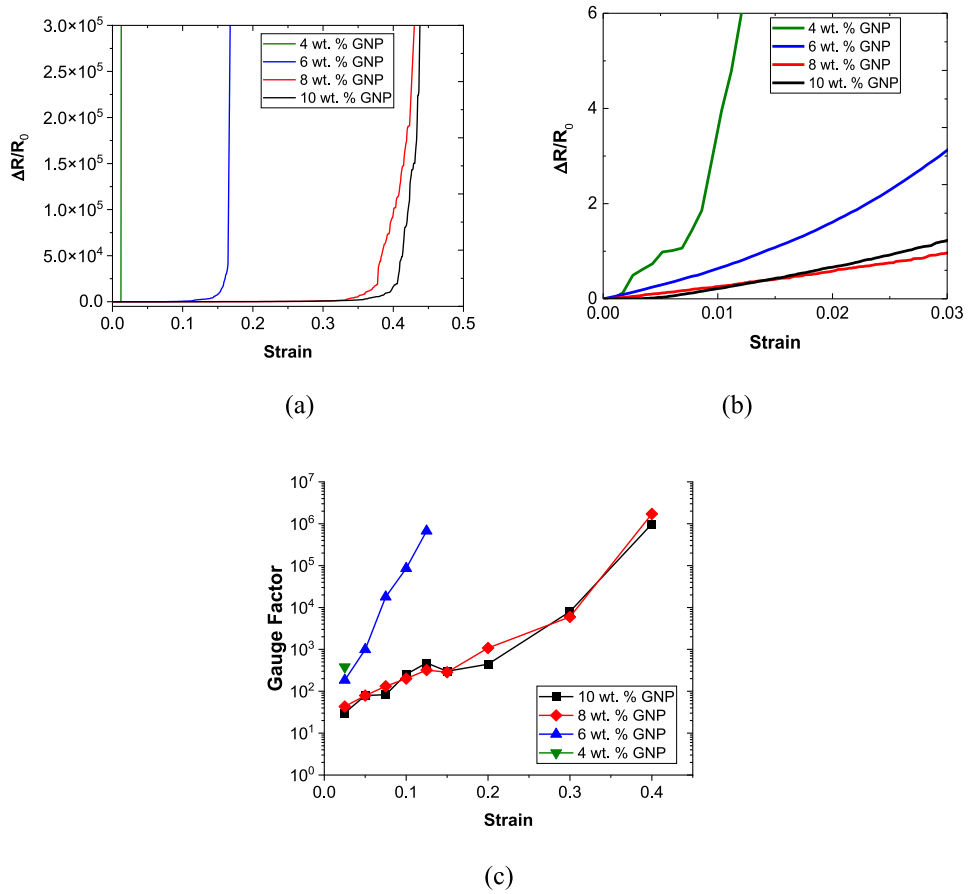

Fig. 4. Strain-sensing response of GNP-PDMS sensors under tensile conditions showing the variation of the normalized resistance with applied strain (a) during all the test and (b) under low values of strain and (c) GF value as a function of applied strain. (A colour version of this figure can be viewed online.)

between neighbouring GNPs, that leads to a reduction in the tunnelling distance (Fig. 5c) and, thus, to a reduction of the electrical resistance associated to this phenomenon. However, when increasing the compressive strain, the out-of-plane mechanisms take a main role in the electrical response of the nanocomposite. Here, due to Poisson's effect, the distance between neighbouring GNPs increases (Fig. 5d), leading, thus, to an increase in the tunnelling resistance [34].

In this regard, Fig. 5e summarizes the GF for the different contents as a function of the applied strain. In this case, a significative reduction of the sensitivity was observed in comparison to the tensile tests, as expected. When comparing the GF values among the different GNP contents a combined effect is observed. On one hand, the samples with the lowest GNP content (4 wt% and 6 wt%) showed the highest sensitivity to compressive strain at the initial stages, as expected due to the higher interparticle distance which induces a higher variation of the electrical resistance of the in-plane mechanisms. When increasing the applied strain, a change in the behaviour was observed and, for medium values of strain level, the highest contents (8 wt% and 10 wt%) also showed the highest sensitivities. This is explained by the change in the prevalent electrical mechanisms from in-plane to out-of-plane mechanisms. At this strain levels, both mechanisms are balanced, so low values of GF are observed for every content. Finally, at the last stages of the compressive tests, the samples with the lowest GNP contents showed again the highest GF, because of the prevalence of the previously mentioned out-of-plane mechanisms, which also depends on the tunnelling distance between neighbouring nanoparticles.

Finally, Fig. 6 shows the electrical response under repetitive tensile and compression cycles to study the stability of the manufactured sensors. The samples with 4 wt% GNPs were not tested as the loss of electrical contact was observed at very low strain levels, as commented before. Moreover, the mechanical response recorded in these tests is shown in Supplementary Information.

Regarding tensile cycling test (Fig. 6a and b), two important facts can be stated: on one hand, the sensitivity under cyclic load at low strain levels ($\varepsilon = 0.01$) is very high (with resistance changes up to 60%) and increases with decreasing GNP content, as expected. On the other hand, some irreversibility in the electrical response can be noticed, especially in the first cycles with a general reduction of the sensitivity. This has been previously observed in other studies [25], and is correlated to the continuous destruction and reconstruction of the GNPs networks during the stretching-releasing process until a stable GNP network is achieved. In any case, the response under cyclic strain was quite stable, proving their potential as wearable sensors.

Regarding compression cycling tests (Fig. 6c and d), a similar

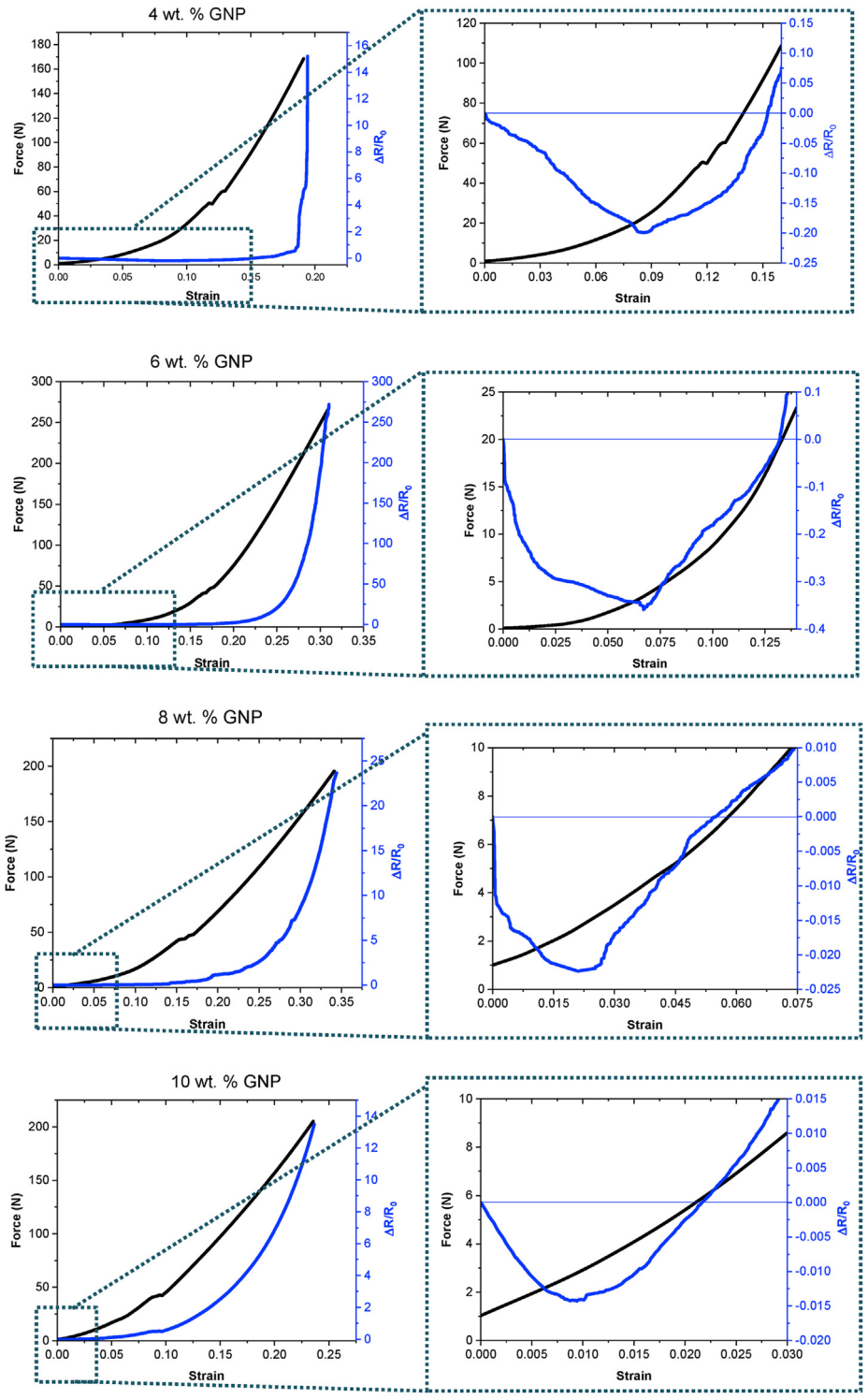

(a)

Fig. 5. (a) Electromechanical response under compressive load for the different GNP-PDMS conditions; schematics of (b) compressive test, (c) in-plane and (d) out-of-plane contacts between neighbouring nanoparticles and (e) GF value as a function of applied strain. (A colour version of this figure can be viewed online.)

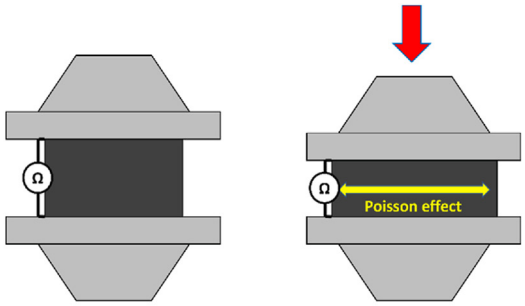

(b)

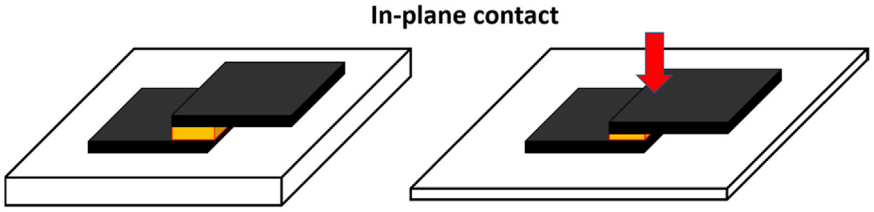

(c)

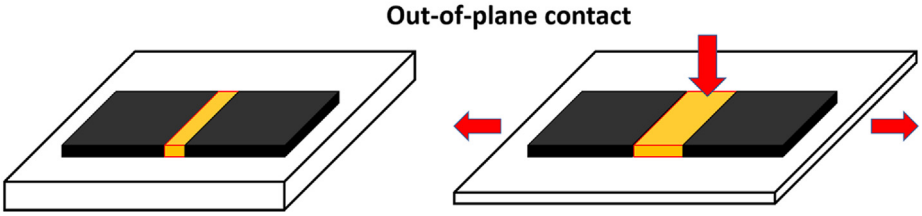

(d)

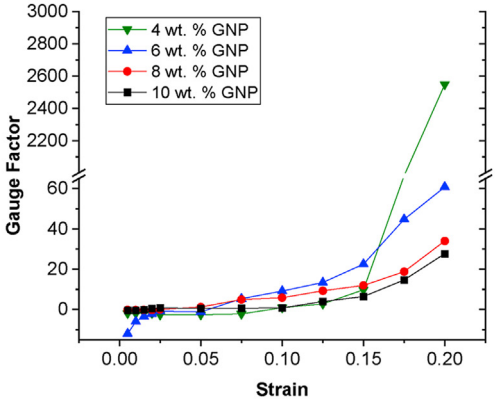

(e)

Fig. 5. (*continued*).

behavior is observed than explained for cycling tensile test. However, the sensitivity at low strain levels ($\varepsilon = 0.01$) is high, but much lower than reported in tensile test, reaching resistance changes up to 10% with 6 wt% GNP nanocomposites. This effect can be explained due to the lower GF in compression conditions, as described above. Furthermore, some irreversibility that is manifested in a progressive decrease in the normalized resistance can be noted in the first cycles since combine effect of the continuous destruction and reconstruction of the GNPs commented before, with the fact that the force applied to achieve the same strain is higher in the first cycles (Fig. S2b of Supplementary Information). After these first cycles, the electrical response showed a much more stable value. Moreover, this irreversibility is quite higher in case of compression cycling tests. This can be explained due to the lower sensitivity at this load condition, leading to a higher prevalence of the irreversible phenomena.

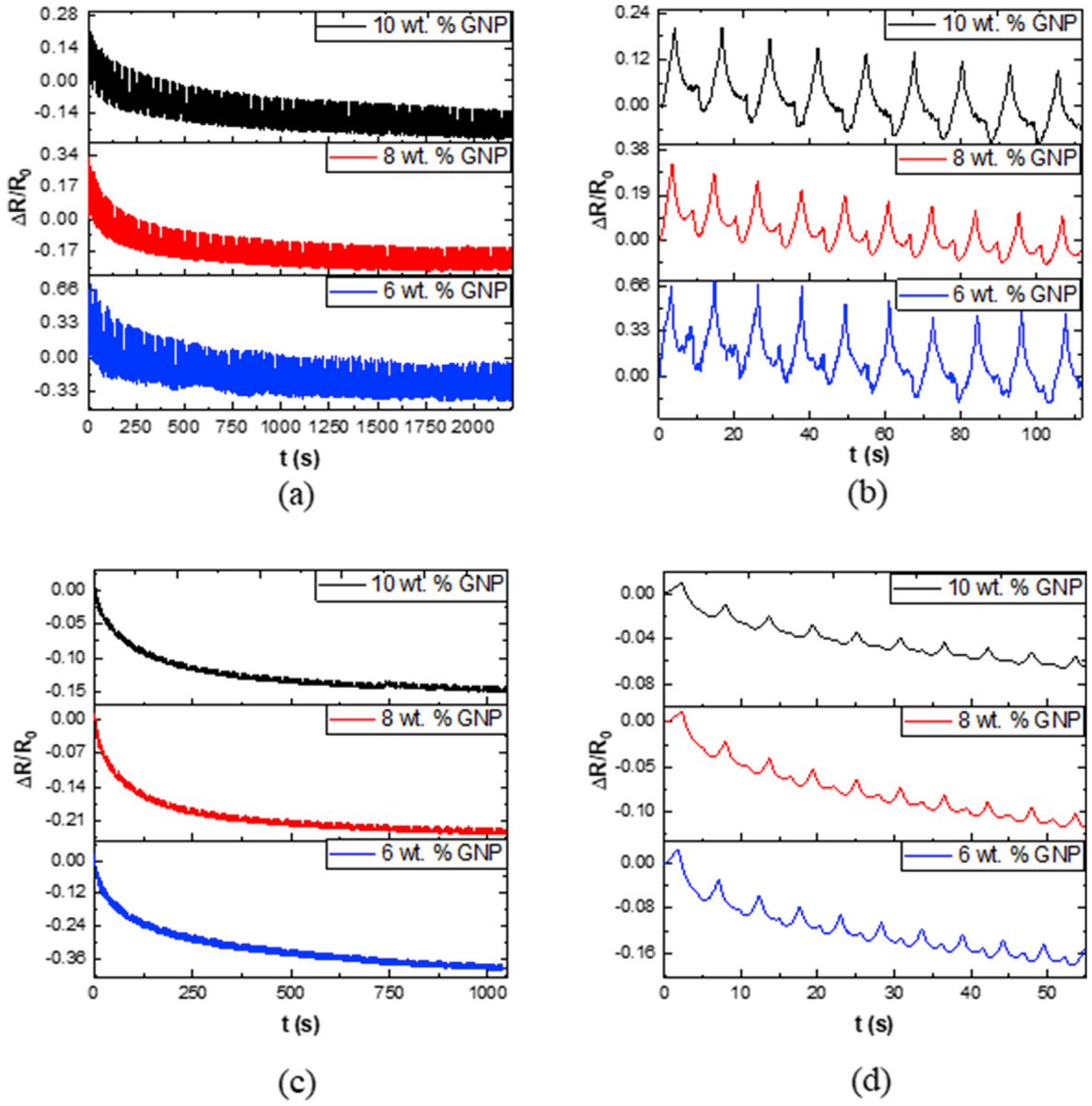

Fig. 6. Electrical response under cyclic load at low strain levels ($\varepsilon = 0.01$). (a) 200 tensile cycles and (b) detail of the first 10 tensile cycles; (c) 200 compression cycles and (d) detail of the first compression 10 cycles. (A colour version of this figure can be viewed online.)

3.3. Complex impedance sensitivity analysis

The analysis of the DC response showed an outstanding sensitivity to applied strain, even at low strain levels. Here, the effect of both GNP content and mechanical strain in the AC response was explored, to better understand the mechanisms that are involved in the electrical response of this type of materials.

In this regard, Fig. 7a shows the EIS results for the different conditions at the pristine state. It can be observed that, by decreasing the content of GNPs, an increase of the complex impedance was achieved. More specifically, when focusing in the EIS response of the 8 and 10 wt% samples (highlighted region of Fig. 7a), a change in the complex impedance behavior from a semicircle to a straight line can be observed.

Here, for a better explanation, it is necessary to understand the electrical mechanisms governing this type of materials. More specifically, the electrical network can be modelled by a series-parallel circuit composed by an RC element, which corresponds to the tunnelling effect occurring between adjacent nanoparticles and an LRC element, corresponding to the intrinsic and contact resistance between nanoparticles. In this regard, this series-parallel circuit can be used to fit the experimental data obtained in the tests (Fig. 7b).

Fig. 8 shows the experimental data and the theoretical predictions by using the previously proposed circuit. It can be observed that it completely fits the experimental measurements, enabling to explain the possible interactions inside the network.

In this context, Table 1 summarizes the values of the electrical resistance corresponding to the RC element, RRC, that is, the resistance associated to the tunnelling effect between neighbouring nanoparticles and to the LRC element, RLRC, that is, the resistance associated to the intrinsic and contact resistance between GNPs. Here, it can be observed that increasing the GNP amount leads to a decrease of the electrical resistance of both RC and LRC elements, due to the creation of more prevalent electrical

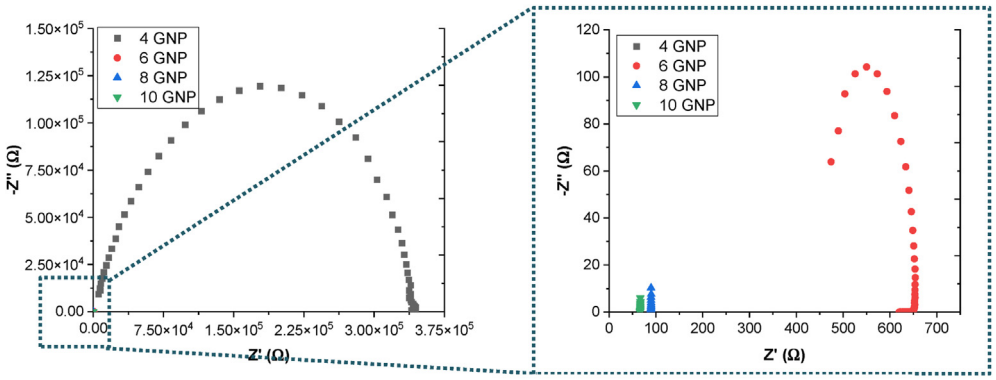

(a)

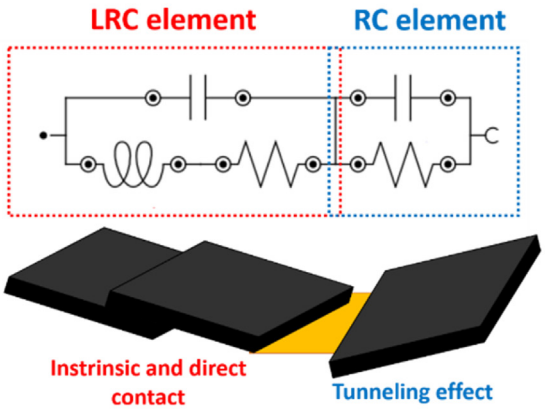

(b)

Fig. 7. (a) EIS curves for the initial state of the different GNP-PDMS sensors and (b) Series-parallel LRC-RC circuit used for fitting the experimental measurements. (A colour version of this figure can be viewed online.)

pathways. More specifically, the reduction in the electrical resistance associated to the LRC element with increasing GNP content is explained by the creation of more electrical contacts between adjacent nanoparticles due to the presence of a higher amount of nanofillers. However, the decrease of the electrical resistance associated to the RC element is explained by a reduction on the mean tunnelling distance between neighbouring nanoparticles.

Furthermore, the effect of a compressive strain on the EIS response was also investigated. In this regard, Fig. 8 also summarizes the EIS analysis as a function of the compressive deformation of the GNP samples. Here, it can be observed that, in general, the compressive deformation leads to a drastic change in the EIS response. A significant increase in the real and imaginary parts of the complex impedance was observed when stretching the sensors. This behaviour is in good agreement with the previously explained electromechanical response under compressive strain. More specifically, when analysing in detail the EIS curves, several facts can be stated.

On one hand, it can be noticed that the electrical resistance of both RC and LRC elements increases with the increasing compressive strain, as also observed in Table 1 This fact is in good agreement with the electromechanical behaviour at compressive strain explained in the previous section, where an increase of the electrical resistance was observed. In this regard, it can be also stated that the ratio between RLRC at pristine state (12 mm) and after maximum compressive deformation (9 mm) increases with the decreasing GNP amount. This fact can be explained by the higher sensitivity of the network to the breakage and creation of electrical contacts when decreasing the number of nanoparticles.

Therefore, the EIS analysis of the complex impedance of the materials at pristine conditions and after deformation, prove the high sensitivity of them under mechanical loading.

3.4. Human motion monitoring

Fig. 9 illustrates different examples of human motion monitoring by using the proposed PDMS sensors in order to prove their high sensitivity.

In this regard, Fig. 9a and b show the electromechanical response when frowning and raising eyebrows. Here, it can be observed that, in both cases, the sensors were perfectly able to detect the motion, with a sudden increase of the electrical resistance. In this context, depending on the motion type, the electrical resistance could present a plateau region, as it was noticed when frowning (Fig. 9a), or several peaks, as it was observed when raising eyebrows (Fig. 9b), explained by the high number of muscles involved in this movement.

Moreover, Fig. 9c shows the electromechanical response when

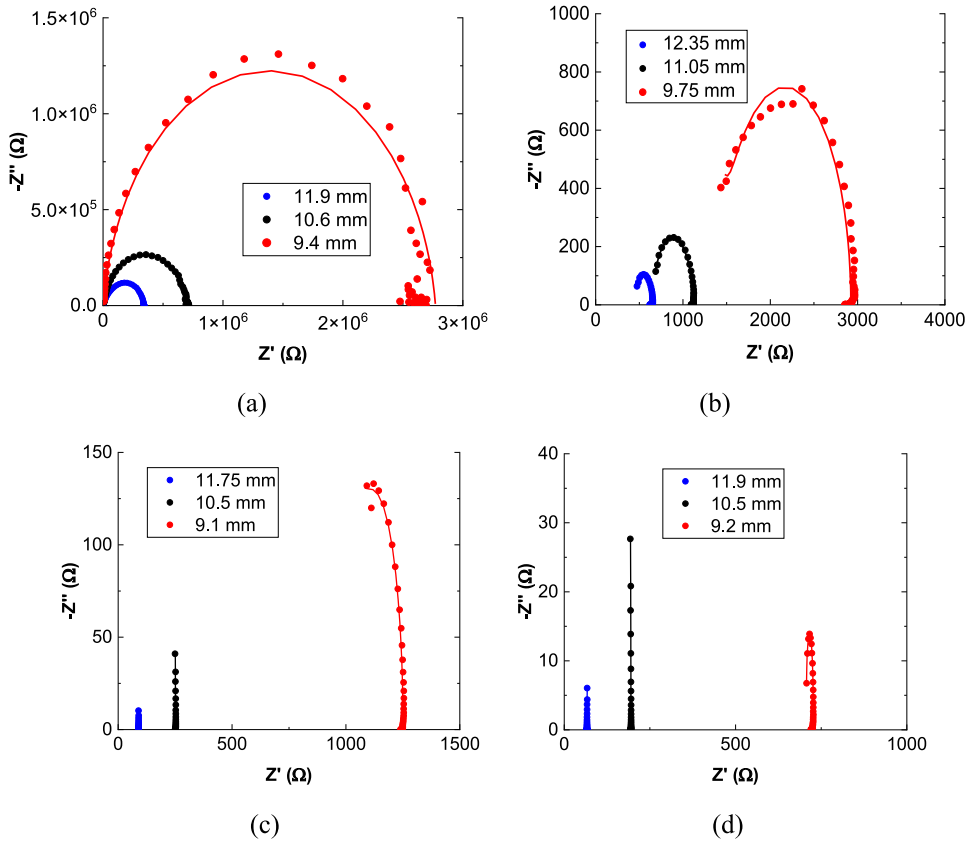

Fig. 8. EIS curves as a function of the compressive deformation for (a) 4, (b), 6, (c) 8 and (d) 10 wt% GNP samples where the dots denote the experimental measurements and the solid lines the fitted data using the equivalent circuit. (A colour version of this figure can be viewed online.)

Table 1
Values of the electrical resistance of the RC and LRC elements.

Condition	*RC element (Ω)*			*LRC element (Ω)*		
	12 mm	10.5 mm	9 mm	12 mm	10.5 mm	9 mm
4% GNP	$335 \cdot 10^3$	$695 \cdot 10^3$	$2650 \cdot 10^3$	$20 \cdot 10^3$	$45 \cdot 10^3$	$252 \cdot 10^3$
6% GNP	455	664	1500	201	450	1410
8% GNP	58,4	183	1080	31.1	69	175
10% GNP	51,3	177	707	15	17.5	20

blinking, where a sudden increase of the electrical resistance was again recorded. It increases accordingly to the intensity of the movement. In addition to that fact, it can be stated that the sensors are able to detect rapid movements, such a quick blinking, as observed in the consecutive peaks at the end of the test.

Furthermore, not only facial motion monitoring was carried out, but the response of the developed sensors was also tested for blowing and breathing sensing, as shown in the graphs of Fig. 9d and e. In both cases, a very sensitive response of the sensors was proved. More specifically, it is possible to distinguish among different intensities when blowing, reflected in a higher (or lower) increase of the electrical response. In case of breathing, the noise of the electrical response was higher. This fact is explained by the complexity of movements involved when breathing, specially at high intensities, where the Adam's apple movement induces a sudden deformation of the sensor.

Finally, a proof of concept of vocal cord's movements was carried out, as shown in the graphs of Fig. 9f. Firstly, the vowels were pronounced one by one and, finally, a short message was said to prove the potential of the developed sensors.

By analysing the graphs of Fig. 9f, it can be observed that the electrical response behaved accordingly to each phoneme pronunciation. For example, when saying “a”, which is pronounced “eɪ”, a double peak in the electrical resistance was observed. The same was also observed when saying “i” (aɪ), whereas a single high peak was recorded when saying “e” (i). In case of “o” and “u”, a single peak was observed with a plateau, corresponding to both phonemes (oʊ and juː). The electrical monitoring of the “S–O–S” message, also show a huge sensitivity, with clear peaks in the electrical resistance corresponding to each letter pronounced. In addition, it can be observed that the shape for each phoneme is unique and always follows a similar pattern, with an increase of the electrical resistance accordingly to the intensity of the voice (higher variations of electrical resistance correspond to higher intensities, as expected). Therefore, the results prove an outstanding robustness of the sensors for vocal cord motion monitoring and could open a wide way for the application of these materials.

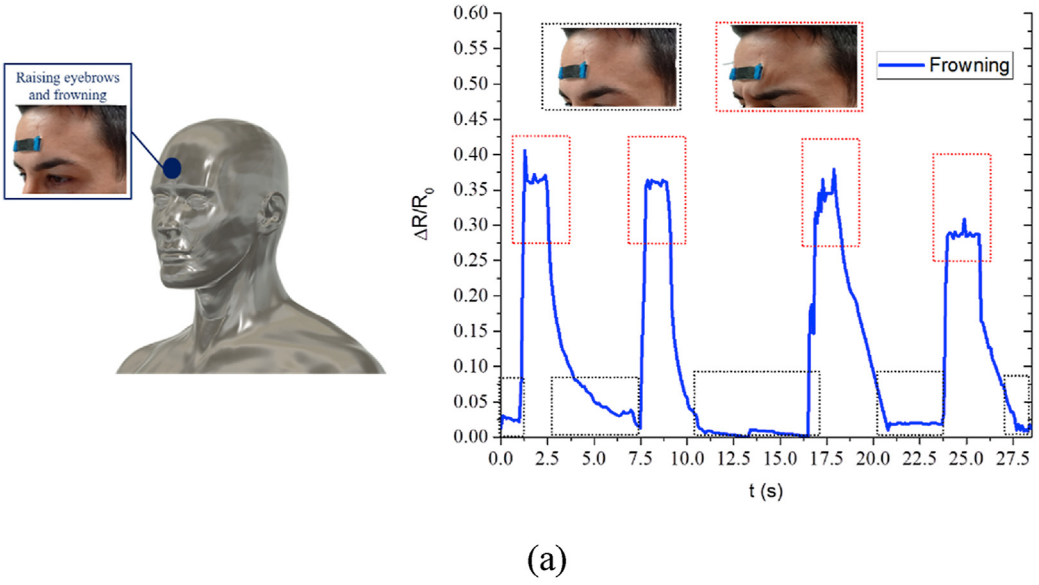

(a)

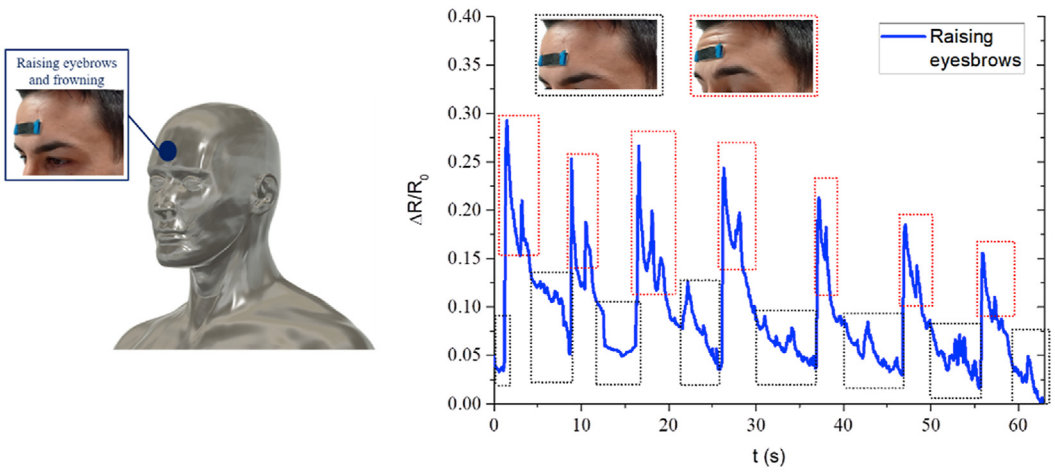

(b)

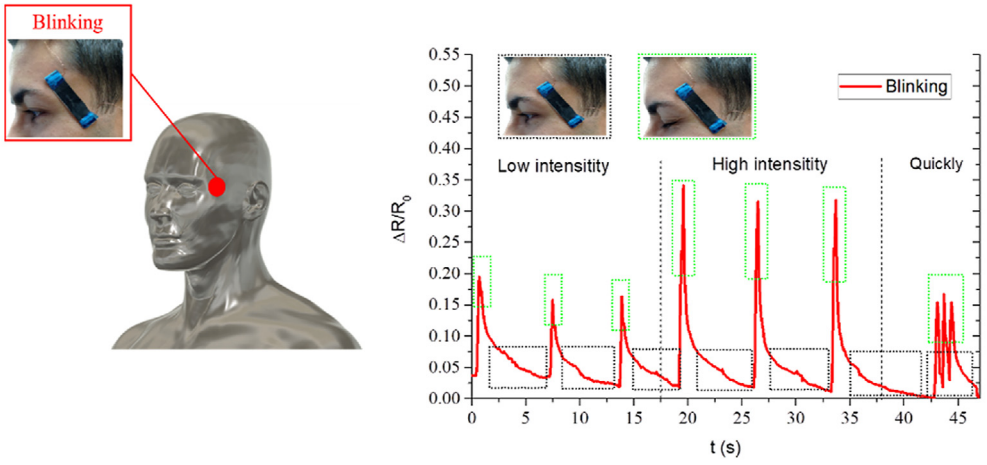

(c)

Fig. 9. Electrical response to human motion when (a) frowning, (b) raising eyebrows, (c) blinking, (d) blowing, (e) breathing and (f) vocal cord monitoring. (A colour version of this figure can be viewed online.)

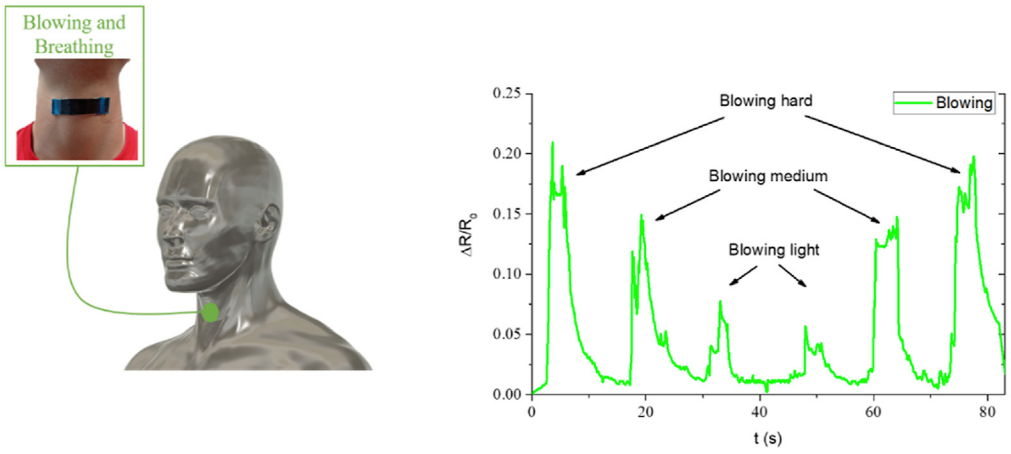

(d)

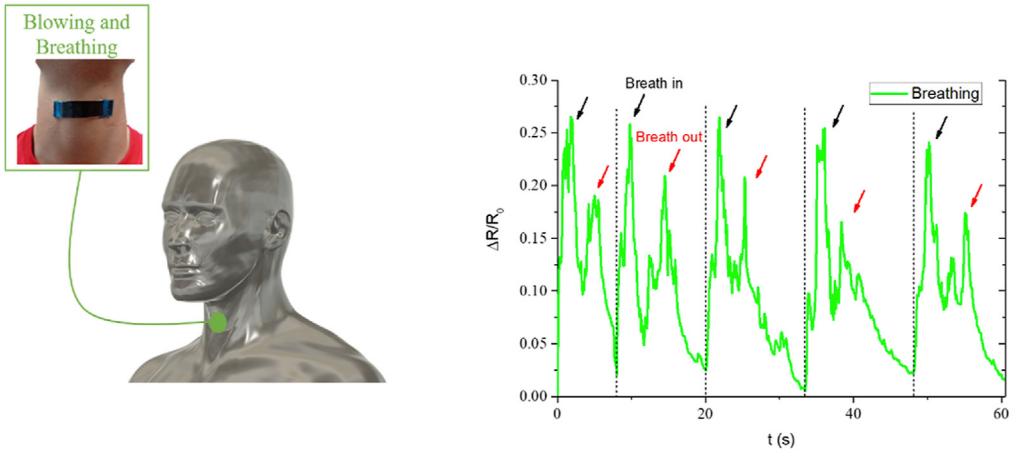

(e)

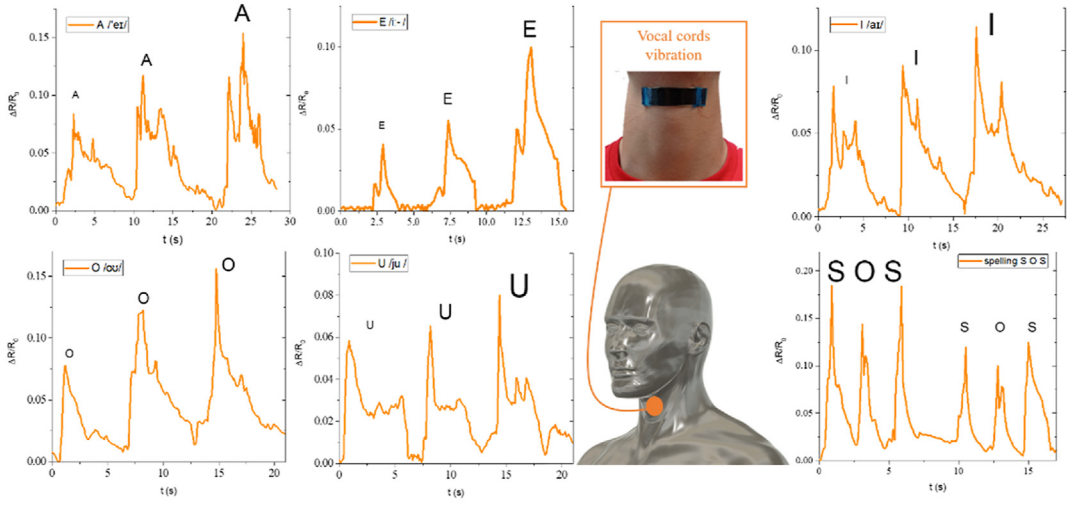

(f)

Fig. 9. (*continued*).

4. Conclusions

The electromechanical and complex impedance response of highly stretchable sensors made of GNP reinforced PDMS was investigated.

The analysis of strain monitoring response showed that an increase of the GNP content leads to a decrease on the sensitivity under tensile conditions due to the reduction in the tunnelling distance between neighbouring nanoparticles. The values of the GF were around 40–300 at low strain levels and up to 10^6 at high strains, proving an enormous sensitivity of the developed sensors. During compression tests, an initial decrease of the electrical resistance was observed, followed by an increase at high strain levels. It was explained by the change in the prevalence of in-plane to out-of-plane mechanisms, governed by tensile strain due to Poisson's effect.

The EIS study was carried out to get a deeper knowledge of strain monitoring mechanisms. Here, the complex impedance response can be modelled by a series RC-LRC circuit, where the first term (RC) denotes the contact and intrinsic and the latter (LRC), the tunnelling mechanisms. In this regard, the EIS analysis under compressive stress showed a very sensitive response, which a significant increase of both resistance and capacitance associated to contact and tunnelling mechanisms.

Finally, a proof of concept of human motion monitoring was carried out. Here, the manufactured sensors were able to detect frowning, blinking, and raising of eyebrows. In addition, their sensitivity is high enough to detect breathing, blowing and vocal cord movements. In the last case, each phoneme is associated to a unique electrical pattern, whose magnitude depends on the intensity of the voice.

Therefore, the proposed GNP/PDMS sensors with a scalable and an easy-manufactured system showed an outstanding potential and applicability for strain-sensing purposes of high and small movements.

CRediT authorship contribution statement

Antonio del Bosque: Conceptualization, Formal analysis, Investigation, Methodology, Writing – original draft. **Xoan F. Sánchez-Romate:** Conceptualization, Formal analysis, Investigation, Writing – original draft. **María Sánchez:** Funding acquisition, Writing – review & editing. **Alejandro Ureña:** Funding acquisition.

Declaration of competing interest

The authors declare that they have no known competing financial interests or personal relationships that could have appeared to influence the work reported in this paper.

Acknowledgment

This work was supported by the Agencia Estatal de Investigación of Spanish Government [Project MULTIFUNC-EVs PID2019-107874RB-I00] and Comunidad de Madrid Government [Project ADITIMAT-CM (S2018/NMT-4411)].

Appendix A. Supplementary data

Supplementary data to this article can be found online at https://doi.org/10.1016/j.carbon.2022.02.043.

References

[1] M. Amjadi, K.-U. Kyung, I. Park, and M. Sitti, "Stretchable, skin-mountable, and wearable strain sensors and their potential applications: a review," Adv. Funct. Mater., vol. 26, no. 11, pp. 1678–1698, Mar. 2016, doi: 10.1002/ADFM.201504755.

[2] A. Mehmood, et al., Graphene based nanomaterials for strain sensor application—a review, J. Environ. Chem. Eng. 8 (3) (Jun. 2020), https://doi.org/10.1016/J.JECE.2020.103743, 103743.

[3] J.K.W. Sandler, J.E. Kirk, I.A. Kinloch, M.S.P. Shaffer, A.H. Windle, Ultra-low electrical percolation threshold in carbon-nanotube-epoxy composites, Polymer 44 (19) (Aug. 2003) 5893–5899.

[4] W. Bauhofer, J.Z. Kovacs, A review and analysis of electrical percolation in carbon nanotube polymer composites, Compos. Sci. Technol. 69 (10) (Aug. 2009) 1486–1498, https://doi.org/10.1016/J.COMPSCITECH.2008.06.018.

[5] C. Li, E.T. Thostenson, T.-W. Chou, Dominant role of tunneling resistance in the electrical conductivity of carbon nanotube–based composites, Appl. Phys. Lett. 91 (22) (Nov. 2007) 223114, https://doi.org/10.1063/1.2819690.

[6] L.M. Chiacchiarelli, M. Rallini, M. Monti, D. Puglia, J.M. Kenny, L. Torre, The role of irreversible and reversible phenomena in the piezoresistive behavior of graphene epoxy nanocomposites applied to structural health monitoring, Compos. Sci. Technol. 80 (May 2013) 73–79, https://doi.org/10.1016/J.COMPSCITECH.2013.03.009.

[7] C. Fang, J. Zhang, X. Chen, G.J. Weng, Calculating the electrical conductivity of graphene nanoplatelet polymer composites by a Monte Carlo method, Nanomater. 2020 (6) (Jun. 2020) 1129, https://doi.org/10.3390/NANO10061129, 10, Page 1129, vol. 10.

[8] X. Li et al., "Large-area ultrathin graphene films by single-step marangoni self-assembly for highly sensitive strain sensing application," Adv. Funct. Mater., vol. 26, no. 9, pp. 1322–1329, Mar. 2016, doi: 10.1002/ADFM.201504717.

[9] G. Shi, et al., Highly sensitive, wearable, durable strain sensors and stretchable conductors using graphene/silicon rubber composites, Adv. Funct. Mater. 26 (42) (Nov. 2016) 7614–7625, https://doi.org/10.1002/ADFM.201602619.

[10] Y. Yf, et al., An ultrasensitive strain sensor with a wide strain range based on graphene armour scales, Nanoscale 10 (24) (Jun. 2018) 11524–11530, https://doi.org/10.1039/C8NR02652A.

[11] U.H. Shin, D.W. Jeong, S.M. Park, S.H. Kim, H.W. Lee, J.M. Kim, Highly stretchable conductors and piezocapacitive strain gauges based on simple contact-transfer patterning of carbon nanotube forests, Carbon N. Y. 80 (1) (Dec. 2014) 396–404, https://doi.org/10.1016/J.CARBON.2014.08.079.

[12] A. M, Y. Yj, P. I, Ultra-stretchable and skin-mountable strain sensors using carbon nanotubes-Ecoflex nanocomposites, Nanotechnology 26 (37) (Sep. 2015), https://doi.org/10.1088/0957-4484/26/37/375501.

[13] S. Zhang, L. Wen, H. Wang, K. Zhu, M. Zhang, Vertical CNT–Ecoflex nanofins for highly linear broad-range-detection wearable strain sensors, J. Mater. Chem. C 6 (19) (May 2018) 5132–5139, https://doi.org/10.1039/C7TC05571D.

[14] Y. Zheng, et al., The effect of filler dimensionality on the electromechanical performance of polydimethylsiloxane based conductive nanocomposites for flexible strain sensors, Compos. Sci. Technol. 139 (Feb. 2017) 64–73, https://doi.org/10.1016/J.COMPSCITECH.2016.12.014. C.

[15] T. Li, et al., A flexible strain sensor based on CNTs/PDMS microspheres for human motion detection, Sensors Actuators, A Phys. 306 (May 2020) 111959, https://doi.org/10.1016/j.sna.2020.111959.

[16] A. del Bosque, X.F. Sánchez-Romate, M. Sánchez, A. Ureña, Flexible wearable sensors based in carbon nanotubes reinforced poly(ethylene glycol) diglycidyl ether (PEGDGE): analysis of strain sensitivity and proof of concept, Chemosensors 9 (7) (Jun. 2021) 158, https://doi.org/10.3390/chemosensors9070158.

[17] N. Lu, C. Lu, S. Yang, J. Rogers, Highly sensitive skin-mountable strain gauges based entirely on elastomers, Adv. Funct. Mater. 22 (19) (Oct. 2012) 4044–4050, https://doi.org/10.1002/ADFM.201200498.

[18] J.-H. Kong, N.-S. Jang, S.-H. Kim, J.-M. Kim, Simple and rapid micropatterning of conductive carbon composites and its application to elastic strain sensors, Carbon N.Y., Chimia 77 (2014) 199–207, https://doi.org/10.1016/J.CARBON.2014.05.022.

[19] P. Song, G. Wang, and Y. Zhang, "Preparation and performance of graphene/carbon black silicone rubber composites used for highly sensitive and flexible strain sensors," Sensors Actuators A Phys., vol. 323, p. 112659, Jun. 2021, doi: 10.1016/J.SNA.2021.112659.

[20] R. Moriche, M. Sánchez, A. Jiménez-Suárez, S. G. Prolongo, and A. Ureña, "Strain monitoring mechanisms of sensors based on the addition of graphene nanoplatelets into an epoxy matrix," Compos. Sci. Technol., vol. 123, pp. 65–70, Feb. 2016, doi: 10.1016/J.COMPSCITECH.2015.12.002.

[21] S. Luo, T. Liu, SWCNT/Graphite nanoplatelet hybrid thin films for self-temperature-compensated, highly sensitive, and extensible piezoresistive sensors, Adv. Mater. 25 (39) (Oct. 2013) 5650–5657, https://doi.org/10.1002/ADMA.201301796.

[22] C.-G. Zhou, et al., Highly stretchable and sensitive strain sensor with porous segregated conductive network, ACS Appl. Mater. Interfaces 11 (40) (Oct. 2019) 37094–37102, https://doi.org/10.1021/ACSAMI.9B12504.

[23] S. Shajari, M. Mahmoodi, M. Rajabian, K. Karan, U. Sundararaj, L.J. Sudak, Highly sensitive and stretchable carbon nanotube/fluoroelastomer nanocomposite with a double-percolated network for wearable electronics, Adv. Electron. Mater. 6 (2) (Feb. 2020) 1901067, https://doi.org/10.1002/AELM.201901067.

[24] S. Wang, Y. Fang, H. He, L. Zhang, C. Li, and J. Ouyang, "Wearable stretchable dry and self-adhesive strain sensors with conformal contact to skin for high-quality motion monitoring," Adv. Funct. Mater., vol. 31, no. 5, p. 2007495, Jan. 2021, doi: 10.1002/ADFM.202007495.

[25] X. Li et al., "A universal method for high-efficiency immobilization of semiconducting carbon nanotubes toward fully printed paper-based electronics," Adv. Electron. Mater., vol. 7, no. 3, p. 2001025, Mar. 2021, doi: 10.1002/AELM.202001025.

[26] Z. Lv, X. Huang, D. Fan, P. Zhou, Y. Luo, and X. Zhang, "Scalable manufacturing of conductive rubber nanocomposites with ultralow percolation threshold for strain sensing applications," Compos. Commun., vol. 25, p. 100685, Jun. 2021, doi: 10.1016/J.COCO.2021.100685.

[27] Y. Wang et al., "Highly stretchable and reconfigurable ionogels with unprecedented thermoplasticity and ultrafast self-healability enabled by gradient-responsive networks," Macromolecules, vol. 54, no. 8, pp. 3832–3844, Apr. 2021, doi: 10.1021/ACS.MACROMOL.1C00443.

[28] Y. Zhan et al., "High sensitivity of multi-sensing materials based on reduced graphene oxide and natural rubber: the synergy between filler segregation and macro-porous morphology," Compos. Sci. Technol., vol. 205, p. 108689, Mar. 2021, doi: 10.1016/J.COMPSCITECH.2021.108689.

[29] X.F. Sánchez-Romate, V. Saiz, A. Jiménez-Suárez, M. Campo, A. Ureña, The role of graphene interactions and geometry on thermal and electrical properties of epoxy nanocomposites: a theoretical to experimental approach, Polym. Test. 90 (Oct. 2020) 106638, https://doi.org/10.1016/J.POLYMERTESTING.2020.106638.

[30] S.G. Prolongo, R. Moriche, A. Jiménez-Suárez, M. Sánchez, A. Ureña, Advantages and disadvantages of the addition of graphene nanoplatelets to epoxy resins, Eur. Polym. J. 61 (Dec. 2014) 206–214, https://doi.org/10.1016/J.EURPOLYMJ.2014.09.022.

[31] X.F. Sánchez-Romate, A. Sans, A. Jiménez-Suárez, M. Campo, A. Ureña, S.G. Prolongo, Highly multifunctional GNP/epoxy nanocomposites: from strain-sensing to joule heating applications, Nanomater. 2020 10 (12) (Dec. 2020) 2431, https://doi.org/10.3390/NANO10122431, 10, Page 2431.

[32] J.G. Simmons, Generalized formula for the electric tunnel effect between similar electrodes separated by a thin insulating film, J. Appl. Phys. 34 (6) (Jun. 2004) 1793, https://doi.org/10.1063/1.1702682.

[33] X.F. Sánchez-Romate, R. Moriche, A. Jiménez-Suárez, M. Sánchez, S.G. Prolongo, A. Ureña, Sensitive response of GNP/epoxy coatings as strain sensors: analysis of tensile-compressive and reversible cyclic behavior, Smart Mater. Struct. 29 (6) (May 2020) 65012, https://doi.org/10.1088/1361-665X/AB8316.

[34] M. Sánchez, R. Moriche, X.F. Sánchez-Romate, S.G. Prolongo, J. Rams, A. Ureña, Effect of graphene nanoplatelets thickness on strain sensitivity of nanocomposites: a deeper theoretical to experimental analysis, Compos. Sci. Technol. 181 (Sep. 2019) 107697, https://doi.org/10.1016/J.COMPSCITECH.2019.107697.